 

***LASERS***

PACS numbers: 42.55.Lt; 42.60.Lh
DOI: 10.1070/QE2007v037n05ABEH013381

# Laser on mixtures of nitrogen with electronegative gases pumped by a transverse discharge from a generator with inductive energy storage: Theory and experiment

A.N. Panchenko, A.I. Suslov, V.F. Tarasenko, A.E. Tel'minov

***Abstract*.** **Lasing and discharge characteristics of a nitrogen laser pumped by a transverse discharge from a generator with an inductive energy storage and a semiconductor current interrupter are investigated experimentally. A numerical model is proposed and the operation of a nitrogen – electronegative gas mixture laser is simulated. It is shown both theoretically and experimentally that admixtures of electronegative gases make it possible to control the laser pulse shape at the $C^3\Pi_u - B^3\Pi_g$ transition of nitrogen. Laser pulses at a wavelength of 337.1 nm, consisting of two peaks, as well as rectangular pulses of duration 40 – 50 ns, are obtained in mixtures of nitrogen with $NF_3$ and $SF_6$ due to an increase in the electron attachment coefficient and an increase in the electric field. The output UV energy is $\sim$ 25 mJ.**

***Keywords***: *UV nitrogen laser, inductive energy storage, transverse discharge pumping, $NF_3$, $SF_6$ admixtures, numerical simulation, rectangular laser pulses.*

## 1. Introduction

An increase in the energy and pulse duration in electric discharge molecular nitrogen lasers, which was reported in [1 – 12] (second positive system, the $C^3\Pi_u - B^3\Pi_g$ electronic bands, the strongest 337.1-nm 0 – 0 and 357.7-nm 0 – 1 transitions), was observed after the addition of electronegative gases to the working mixture. This effect is manifested most strongly in transverse-discharge-pumped lasers. For practical applications, of interest are UV nitrogen lasers emitting tens of millijoules. However, no numerical model was developed for nitrogen – electronegative gas mixture lasers, which hampered an investigation of processes determining the lasing parameters, as well as the prediction of the working parameters of new lasers. In particular, it was necessary to find the reason behind the generation of laser pulses with two peaks [11, 12]. Theoretical models of a nitrogen laser without any admixtures of electronegative gases, including the model of the atmospheric-pressure nitrogen laser [15 – 17], had been worked out earlier [13 – 17]. In these computations, the electron energy distribution function (EEDF) in nitrogen was assumed to be Maxwellian, which is not true for discharge calculations in mixtures of nitrogen with halogens.

The aim of this paper is to develop a theoretical model of a nitrogen – electronegative gas mixture laser and to study the operation conditions of electric discharge nitrogen lasers excited by the transverse discharge from a generator with an inductive energy storage and SOS diodes, which leads to the formation of laser pulses consisting of several peaks and the attainment of maximum radiation energy.

**A.N. Panchenko, A.I. Suslov, V.F. Tarasenko, A.E. Tel'minov**
Institute of High Current Electronics, Siberian Branch, Russian Academy of Sciences, prosp. Akademicheskii 2/3, 634055 Tomsk, Russia;
e-mail: alexei@loi.hcei.tsc.ru, suslov@to.hcei.tsc.ru

Received 5 September 2006
*Kvantovaya Elektronika* **37** (5) 433 – 439 (2007)
Translated by Ram Wadhwa

## 2. Experimental

We studied a transverse-discharge-pumped laser with spark preionisation, which is described in detail in [11, 18]. A universal generator, capable of excitation from an inductive as well as a capacitive energy storage, was used for pumping. The generator consisted of a spark gap, as well as storage ($C_0 = 70$ nF) and peaking ($C_1 = 2.45$ nF) capacitors. In the inductive storage regime, 10 SOS diodes were connected in parallel to the capacitor $C_1$, and current from an auxiliary capacitor was first passed in the forward direction through them. The use of an inductive storage resulted in shortening of voltage and pump pulses and in the increase in the breakdown voltage and pump power. An aluminium-coated plane mirror and a plane – parallel quartz plate were used as the cavity mirrors. The laser had the active volume $V = 2 \times 4 \times 72$ cm$^3$ (discharge gap $d = 4$ cm).

The output energy of the nitrogen laser was measured with an OPHIR calorimeter with FL-250A and PE-50BB heads. The laser pulse was detected with a FEK-22 SPU vacuum photodiode on which a part of laser radiation was directed by a beamsplitter. The laser emission spectrum was recorded with a StellarNet EPP2000-C25 spectrometer. To provide the operation of the photodiode and spectrometer in the linear regime, the incident radiation was attenuated by metal grids.

The discharge current and voltage across the laser electrodes were detected with a voltage divider and a Rogowski loop. Electric signals were fed to the TDS-220 or TDS-224 oscilloscopes.

## 3. Characteristics of nitrogen – halogen mixture lasers

Figure 1 shows the dependences of the output energy $Q$ of a nitrogen laser on the charge voltage $U_0$ of capacitor $C_0$ for various mixtures under different pump conditions. The optimal pressure of nitrogen in our experiments was 75 Torr. The maximum laser output energy (25 mJ) was achieved in mixtures of nitrogen with $NF_3$ or $SF_6$ and upon pumping by a generator with an inductive storage. The main part of energy was emitted at 337.1 nm, while the fraction of laser radiation energy at 357 nm did not exceed 10 %, as in [11]. In addition, after the end of the UV laser pulse, high-intensity emission was observed in nitrogen–halogen mixtures in the first positive nitrogen system (the $B^3\Pi_g - A^3\Sigma_u^+$ transition with the highest intensity line at 1048 nm). The IR radiation energy for a mixture with $SF_6$ was 5 mJ, which corresponds to the maximum energy obtained at this wavelength upon transverse-discharge pumping [19]. In the $N_2 - F_2$ mixture, the UV radiation energy decreased to 15 mJ.

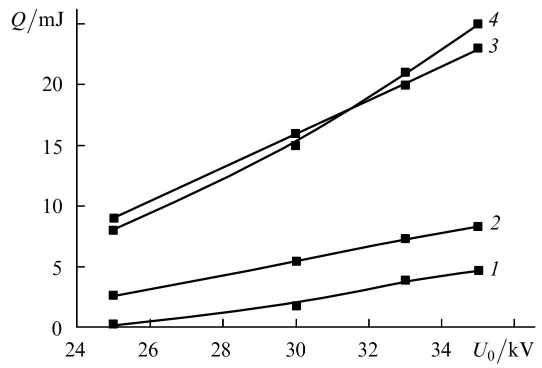


**Figure 1.** Dependences of the output energy $Q$ of a nitrogen laser on the charging voltage $U_0$ of the capacitor $C_0$ in the case of pumping of pure nitrogen by a generator with capacitive (*1*) and inductive (*2*) storage devices, as well as in the case of pumping of mixtures $N_2:NF_3 = 75:3$ Torr (*3*) and $N_2:SF_6 = 75:9$ Torr (*4*) by a generator with an inductive storage device.

Figure 2 shows the oscillograms of the voltage across the laser gap, the discharge current, and laser radiation generated upon pumping pure nitrogen in discharges fed by generators of different kinds. The replacement of the capacitive storage by an inductive storage resulted in the increase in the breakdown voltage. Besides, the discharge current increases sharply during voltage drop across the gap. These factors lead to a considerable increase in the output energy of the nitrogen laser.

A characteristic feature of the nitrogen–$NF_3$ mixture laser operation is the appearance of a second lasing peak in certain pump regimes (Fig. 3). The delay between the laser pulse peaks was $\sim 25$ ns. The double-peak lasing was observed at maximum radiation energies. As $U_0$ was decreased, the ratio of amplitudes of the first and second lasing peaks increased, and the second peak disappeared for low charge voltages. When $SF_6$ was added to nitrogen, the second peak appeared only for $SF_6$ concentrations exceeding 50 %. In this case, the output energy did not exceed 10 mJ, and the laser pulse duration at the base was $\sim$ 50 ns.

An interesting result was obtained upon pumping of nitrogen mixtures with $NF_3$ or $SF_6$ at a lower total pressure of the gas mixture. In this case, the second lasing peak increased and the dip between the peaks in the intensity distribution decreased. This resulted in the formation of rectangular peaks of duration about 50 ns.

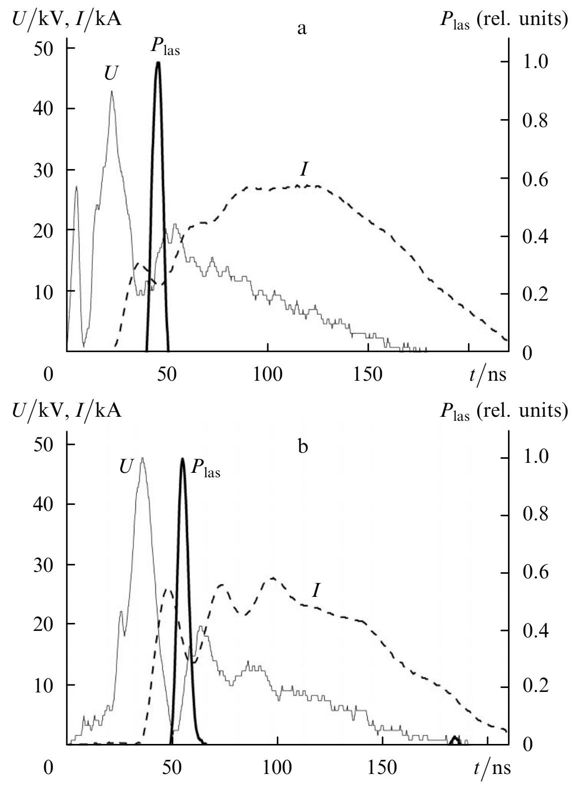


**Figure 2.** Oscillograms of voltage pulses $U$ across the discharge gap, discharge current $I$ and laser pulses $P_{las}$ at $\lambda = 337.1$ nm in pure nitrogen ($p = 75$ Torr) pumped by a capacitive (a) and inductive (b) energy storage device; $U_0 = 35$ kV.

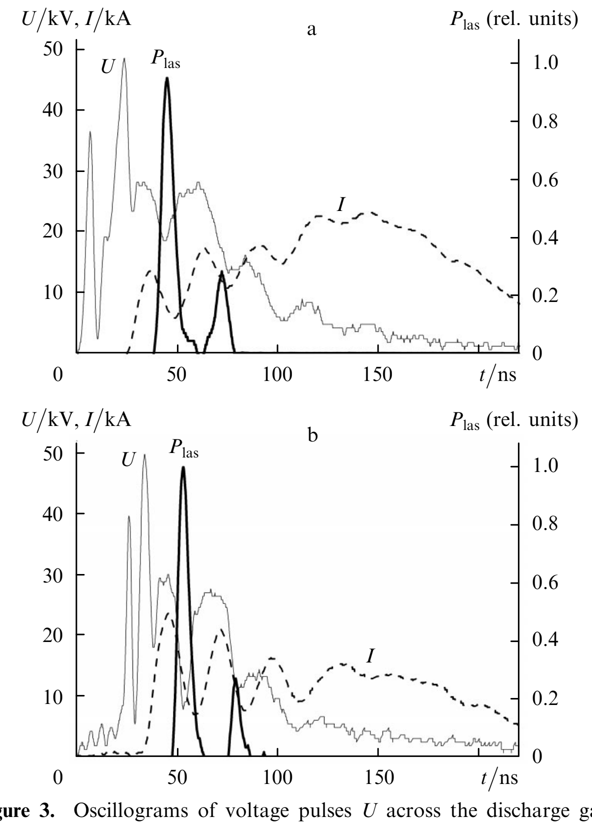


**Figure 3.** Oscillograms of voltage pulses $U$ across the discharge gap, discharge current $I$, and laser pulses $P_{las}$ at $\lambda = 337.1$ nm in the mixture $N_2:NF_3 = 75:3$ Torr pumped by a capacitive (a) and inductive (b) energy storage device; $U_0 = 35$ kV.

## 4. Numerical simulation of a nitrogen laser pumped by a self-sustained discharge in mixtures of $N_2$ with electronegative gases

We simulated plasma-chemical processes in the discharge gap and lasing at the $C^3\Pi_u \rightarrow B^3\Pi_g$ transition by performing the following calculations:

(i) calculation of the electron energy distribution function $f_e(E/p, \varepsilon, t)$ in a self-sustained discharge, where $E$ and $p$ are the electric field strength and gas pressure in the discharge gap, $\varepsilon$ is the electron energy, and $t$ is the time;

(ii) calculation of the physical parameters of electrons (mobility $\mu_e$, temperature $T_e$, diffusion coefficient $D_e$) and the rate constants of the reaction between electrons and plasma particles;

(iii) calculation of the kinetics of heavy particles;

(iv) calculation of the formation of laser radiation in the cavity; and

(v) electrical engineering calculations (laser pumping scheme).

All these calculations in the form of individual program blocks were combined into a self-consistent model, which is presented schematically in Fig. 4.

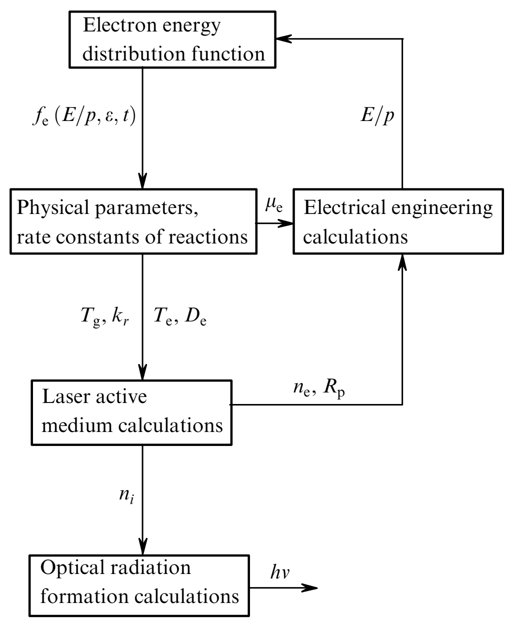


**Figure 4.** Self-consistent model of a plasma chemical reactor [$f_e(E/p, \varepsilon, t)$ is the electron energy distribution function, $\mu_e$ and $D_e$ are the mobility and electron diffusion coefficient, $R_p$ is the discharge plasma resistance, $T_g$ is the gas temperature, $k_r$ is the rate constant of the $r$th reaction; $n_i$ is the concentration of the $i$th particle; and $n_e$ and $T_e$ are the electron concentration and temperature].

The EEDF in a self-sustained discharge in the $N_2 - NF_3$ or $N_2 - SF_6$ mixture was calculated by numerical integration of the Boltzmann equation by using the iterative procedure [20]. The cross section of elementary processes of interaction of electrons with $N_2$, $NF_3$ and $SF_6$ molecules and the rate constants of reactions are borrowed from [21–27].

To determine the concentration of particles in the plasma, we solved numerically the system of kinetic equations for a spatially homogeneous discharge [15]:

$$\frac{dn_i}{dt} = \sum_r \delta_{ir} k_r \prod_{j=1}^{m^{(r)}} \left(n_j^{(r)}\right)^{v_j^{(r)}}, \qquad (1)$$

where $n_i$ is the concentration of the $i$th particle in the active medium of the laser, $\delta_{ir}$ is the difference in the stoichiometric coefficients for the $i$th particle on the left and right sides of the equation for the rth reaction, $n_j^{(r)}$ is the concentration of the $j$th particle participating in the $r$th reaction, $m^{(r)}$ is the number of particles of different species on the left-hand side of the equation for the $r$th reaction, and $v_j^{(r)}$ is the stoichiometric coefficient for the $j$th particle on the left-hand side of the equation for the $r$th reaction. The kinetic scheme of plasma chemical reactions and processes in mixtures of nitrogen with $NF_3$ and $SF_6$ in a self-sustained discharge are presented in Table 1.

**Table 1.** Kinetic diagrams of nonequilibrium plasma-chemical processes in the $N_2 - NF_3$ or $N_2 - SF_6$ mixtures. The data on rate constants of reactions and cross sections are borrowed from [21–27] or calculated (for rate constants of reactions of electrons with neutral and charged particles).

| Reactions | Rate constants |
|---|---|
| 1. Excitation of electron states and ionisation | |
| 1. $N_2 + e \rightarrow N_2(A^3\Sigma_u^+) + e$ | Calculated from EEDF |
| 2. $N_2 + e \longrightarrow N_2(W^3, B') + e$; $\nearrow N_2(B^3\Pi_g) + e$; $\searrow N_2(B^3\Pi_g) + e$ | –"– |
| 3. $N_2 + e \longrightarrow N_2(a, w^1) + e$; $\nearrow N_2(a') + e$; $\searrow N_2(a') + e$ | –"– |
| 4. $N_2 + e \longrightarrow N_2(E, a'') + e$; $\nearrow N_2(C^3\Pi_u) + e$; $\searrow N_2(C^3\Pi_u) + e$ | –"– |
| 5. $N_2 + e \rightarrow N(^4S) + N(^4S) + e$ | –"– |
| 6. $N_2 + e \rightarrow N(^4S) + N(^2D) + e$ | –"– |
| 7. $N_2 + e \rightarrow N(^4S) + N(^2P) + e$ | –"– |
| 8. $N(^4S) + e \rightarrow N(^2D) + e$ | –"– |
| 9. $N(^4S) + e \rightarrow N(^2P) + e$ | –"– |
| 10. $N(^4D) + e \rightarrow N(^2P) + e$ | –"– |
| 11. $N_2 + e \rightarrow N_2^+ + e + e$ | –"– |
| 2. Associative ionisation | |
| 12. $N_2(A^3\Sigma_u^+) + N_2(a') \rightarrow N_4^+ + e$ | $k_{12} \approx 5 \times 10^{-11}$ cm$^3$ s$^{-1}$ |
| 13. $N_2(a') + N_2(a') \rightarrow N_4^+ + e$ | $k_{13} \approx 2 \times 10^{-10}$ cm$^3$ s$^{-1}$ |
| 14. $N(^2D) + N(^2P) \rightarrow N_2^+ + e$ | $k_{14} \approx 10^{-12}$ cm$^3$ s$^{-1}$ |
| 3. Recombination of electrons and positive ions | |
| 15. $N_4^+ + e \rightarrow N_2 + N_2$ | $k_{15} = 2 \times 10^{-6}(300\,K/T_e)$ cm$^3$ s$^{-1}$ |
| 16. $N_3^+ + e \rightarrow N_2(B^3\Pi_g) + N$ | $k_{16} = 10^{-10}$ cm$^3$ s$^{-1}$ |
| 17. $N_2^+ + e \rightarrow N + N$ | $k_{17} = 2.8 \times 10^{-7}(300\,K/T_e)^{1/2}$ cm$^3$ s$^{-1}$ |
| 18. $N_2^+ + e \rightarrow N + N(^2D)$ | $k_{18} = 2 \times 10^{-7}(300\,K/T_e)^{1/2}$ cm$^3$ s$^{-1}$ |
| *Electron–ion recombination (three-body processes)* | |
| 19. $e + e + N_2^+ \rightarrow e + N_2$ | $k_{19} = 10^{-19}(300\,K/T_e)^{4.5}$ cm$^6$ s$^{-1}$ |
| 20. $e + N_2^+ + N_2 \rightarrow 2N_2$ | $k_{20} = 6 \times 10^{-27}(300\,K/T_e)^{1.5}$ cm$^6$ s$^{-1}$ |
| 4. Electron attachment and detachment processes | |
| 21. $e + NF_3 \rightarrow NF_2 + F^-$ | Calculated from EEDF |
| 22. $e + F^- \rightarrow F + 2e$ | –"– |

*(Continued on the next page)*

| | | |
|---|---|---|
| 23. | $e + SF_6 + M \to SF_6^- + M$ | –"– |
| 24. | $e + SF_6 \to SF_5^- + F$ | –"– |
| 25. | $e + SF_6^- \to SF_6 + 2e$ | –"– |
| 26. | $e + SF_5^- \to SF_5 + 2e$ | –"– |
| | 5. Processes involving electronically-excited particles | |
| 27. | $N_2(A^3\Sigma_u^+) + N_2(A^3\Sigma_u^+) \to N_2(C^3\Pi_u) + N_2(X)$ | $k_{27} \simeq 1.6 \times 10^{-10} \times (300\,K/T_g)^{2.64}$ cm$^3$ s$^{-1}$ |
| 28. | $N_2(A^3\Sigma_u^+) + N_2 \to N_2(X) + N_2$ | $k_{28} = 3 \times 10^{-18}$ cm$^3$ s$^{-1}$ |
| 29. | $N_2(A^3\Sigma_u^+) + N(^4S) \to N_2(X) + N(^2P)$ | $k_{29} = 5 \times 10^{-11}$ cm$^3$ s$^{-1}$ |
| 30. | $N_2(A^3\Sigma_u^+) + SF_6 \to N_2(X) + SF_6$ | $k_{30} = 1 \times 10^{-14}$ cm$^3$ s$^{-1}$ |
| 31. | $N_2(A^3\Sigma_u^+) + NF_3 \to N_2(X) + NF_3$ | $k_{31} = 2 \times 10^{-13}$ cm$^3$ s$^{-1}$ |
| 32. | $N_2(B^3\Pi_g) + N_2 \to N_2(A^3\Sigma_u^+) + N_2$ | $k_{32} = 5 \times 10^{-11}$ cm$^3$ s$^{-1}$ |
| 33. | $N_2(B^3\Pi_g) \to N_2(A^3\Sigma_u^+) + h\nu$ | $k_{33} = 1.5 \times 10^5$ s$^{-1}$ |
| 34. | $N_2(a') + N_2 \to N_2(B^3\Pi_g) + N_2$ | $k_{34} \simeq 2 \times 10^{-13}$ cm$^3$ s$^{-1}$ |
| 35. | $N_2(C^3\Pi_u) \to N_2(B^3\Pi_g) + h\nu$ | $k_{35} = 3 \times 10^7$ s$^{-1}$ |
| 36. | $N_2(C^3\Pi_u) + N_2 \to N_2(a') + N_2$ | $k_{36} = 10^{-11}$ cm$^3$ s$^{-1}$ |
| 37. | $N_2(C^3\Pi_u) + SF_6 \to N_2(X) + SF_6$ | $k_{37} = 1.1 \times 10^{-10}$ cm$^3$ s$^{-1}$ |
| 38. | $N_2(C^3\Pi_u) + NF_3 \to N_2(X) + NF_3$ | $k_{38} = 10^{-10}$ cm$^3$ s$^{-1}$ |
| 39. | $N(^2D) + N_2 \to N(^4S) + N_2$ | $k_{39} = 6 \times 10^{-15}$ cm$^3$ s$^{-1}$ |
| 40. | $N(^2P) + N_2 \to N(^2D) + N_2$ | $k_{40} = 2 \times 10^{-18}$ cm$^3$ s$^{-1}$ |
| 41. | $N(^2P) + N \to N(^2D) + N$ | $k_{41} = 1.8 \times 10^{-12}$ cm$^3$ s$^{-1}$ |
| | 6. Ion conversion | |
| 42. | $N_2^+ + N_2 + N_2 \to N_4^+ + N_2$ | $k_{42} = 5 \times 10^{-29}$ cm$^6$ s$^{-1}$ |
| 43. | $N_2^+ + N + N_2 \to N_3^+ + N_2$ | $k_{43} = 0.9 \times 10^{-30} \times \exp(400\,K/T_g)$ cm$^6$ s$^{-1}$ |
| 44. | $N^+ + N_2 + N_2 \to N_3^+ + N_2$ | $k_{44} = 0.9 \times 10^{-29} \times \exp(400\,K/T_g)$ cm$^6$ s$^{-1}$ |
| 45. | $N^+ + N + M \to N_2^+ + M$ $(M = N_2)$ | $k_{45} = 10^{-29}$ cm$^6$ s$^{-1}$ |
| 46. | $N_2^+ + N_2(A^3\Sigma_u^+) \to N_3^+ + N$ | $k_{46} < 3 \times 10^{-10}$ cm$^3$ s$^{-1}$ |
| 47. | $N_2^+ + N \to N^+ + N_2$ | $k_{47} = 2.4 \times 10^{-15} T_g$ cm$^3$ s$^{-1}$ |
| 48. | $N_3^+ + N \to N_2^+ + N_2$ | $k_{48} = 6.6 \times 10^{-11}$ cm$^3$ s$^{-1}$ |
| 49. | $N_4^+ + N_2 \to N_2^+ + N_2 + N_2$ | $k_{49} = 2.5 \times 10^{-15}$ cm$^3$ s$^{-1}$ |
| 50. | $N_4^+ + N \to N^+ + N_2 + N_2$ | $k_{50} = 10^{-11}$ cm$^3$ s$^{-1}$ |
| | 7. Photon emission processes | |
| 51. | $N_2(C^3\Pi_u) \to N_2(B^3\Pi_g) + h\nu$ | $k_{51} = 3 \times 10^7$ s$^{-1}$ |
| 52. | $N_2(C^3\Pi_u) + h\nu \to N_2(B^3\Pi_g) + 2h\nu$ | $\sigma = 7.3 \times 10^{-16}$ cm$^2$ |

Note: $T_e$ and $T_g$ are the electron and gas temperatures.

Figure 5 shows the electric circuit diagram for feeding the discharge used in our calculations. The system of equations for electric circuit calculations has the form

$$L_0 \frac{dI_0}{dt} = U_0 - U_1, \tag{2}$$

$$C_0 \frac{dU_0}{dt} = I_0, \tag{3}$$

$$L_1 \frac{dI_1}{dt} = U_1 - I_1 R_p, \tag{4}$$

and

$$C_1 \frac{dU_1}{dt} = I_0 - I_1. \tag{5}$$

Here, $U_0$ and $U_1$ are the voltages across the storage capacitor $C_0$ and the peaking capacitor $C_1$, respectively; $I_0$ and $I_1$ are the currents in the storage and peaking circuits, respectively; and $R_p$ is the resistance of the electric discharge plasma.

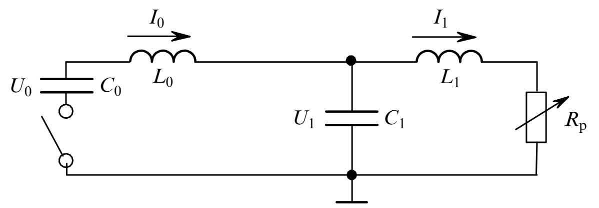


**Figure 5.** Electric circuit diagram for discharge feeding used in the simulations of a nitrogen laser ($C_0 = 70$ nF, $C_1 = 2.45$ nF are the capacitances of storage and peaking capacitors; $L_0 = 25$ nH, $L_1 = 12$ nH are the circuit inductances, $U_0$ and $U_1$ are the voltages across the capacitors $C_0$ and $C_1$; $I_0$ and $I_1$ are the currents through $C_0$ and the load respectively).

The laser radiation kinetics was calculated by using the equation for the photon density $n_{ph}$ in the optical cavity in the approximation of homogeneous distribution of particles over the active medium volume:

$$\frac{dn_{ph}}{dt} = \Omega \frac{n_C}{\tau_{sp}} + c\sigma n_{ph}(n_C - n_B)\frac{l_a}{L} + cn_{ph}\frac{\ln(r_1 r_2)}{2L}, \tag{6}$$

where $n_C$ and $n_B$ are the populations of the upper and lower laser levels, respectively; $\Omega$ is the fraction of spontaneous radiation incident on the output mirror; $r_1$ and $r_2$ are the reflectivities of the resonator mirrors; $l_a$ and $L$ are the lengths of the active region and the optical cavity, respectively; $c$ is the speed of light; $\sigma$ is the cross section of induced photon emission; and $\tau_{sp}$ is the spontaneous lifetime of the upper laser level.

## 5. Discussion of the results of numerical calculations and comparison with the experiment

Numerical calculations of the nitrogen laser operation were performed and compared with the experiments for nitrogen and the $N_2:NF_3 = 25:1$ mixture at $p = 78$ Torr and $U_0 = 35$ kV. Figure 6 shows the calculation oscillograms for the discharge current and voltage across the laser gap, as well as laser pulses for this mixture and pure nitrogen at $p = 75$ Torr. A comparison of Figs 2, 3 and 6 shows a good agreement between the theoretical and experimental curves. The calculated radiation energy is also close to experimental values presented in Fig. 1. One can see from the figures that the voltage across the laser gap in the quasi-stationary discharge stage in pure nitrogen is about half the value for the $N_2 - NF_3$ mixture, and the addition of an electronegative impurity gives rise to the second laser pulse during the quasi-stationary discharge stage. In this regime, the maximum output energy is achieved.

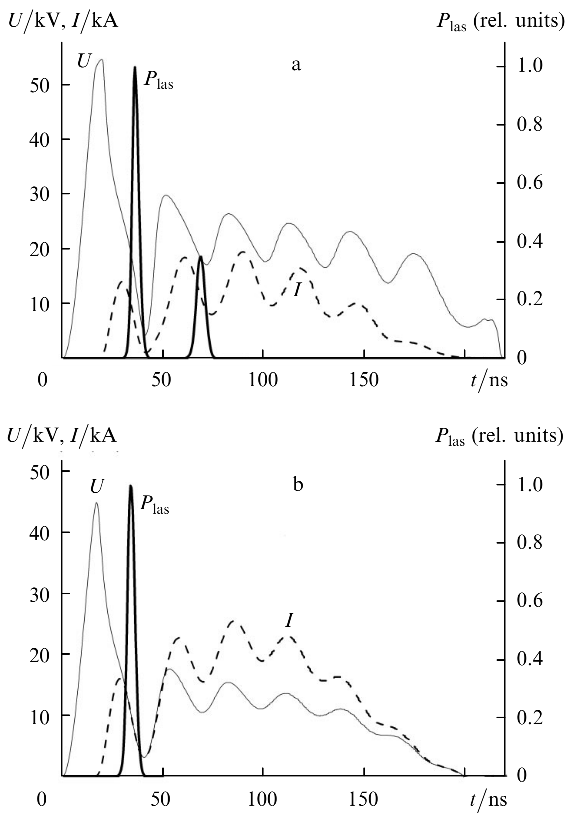


**Figure 6.** Theoretical pulse shapes of voltage $U$ across the discharge gap, discharge current $I$ and laser radiation power $P_{las}$ in the mixture $N_2 - NF_3$ (a) and in pure nitrogen (b).

An increase in the voltage during the quasi-stationary discharge stage after the addition of $NF_3$ is explained by the behaviour of the cross section for electron attachment to $NF_3$. The dependence of the cross section on the electron energy has a maximum at $\sim 2$ eV [26]. Because the average electron energy in the self-sustained discharge in nitrogen is also $\sim 2$ eV, the rate constant of electron attachment to $NF_3$ achieves a maximum value of $8 \times 10^{-9}$ cm$^3$ s$^{-1}$.

Our calculations show that the addition of $NF_3$ to nitrogen for a given voltage across the gap affects the output radiation in two ways. On the one hand, an increase in the voltage across the gap at the quasi-stationary discharge stage results in an increase in the rate of excitation of the upper laser level and hence in the power and duration of laser pulses. On the other hand, the wave impedance of the peaking circuit and the load in the two-circuit power supply are mismatched, which results in the attenuation of the voltage oscillations across the gap due to charge exchange between $C_1$ and $C_0$. The amplitude of these oscillations is sufficient to create periodically in the active medium of the nitrogen laser a state with the inverse population of levels in the $C^3\Pi_u \rightarrow B^3\Pi_g$ transition. As a result, two laser pulses are formed during one pump pulse. Similar voltage oscillations are also observed in pure nitrogen; however, the mean value of the parameter $E/p <$ 30 kV cm$^{-1}$ atm$^{-1}$ at the quasi-stationary discharge stage without an electronegative impurity is insufficient for obtaining the inverse population.

Other electronegative gases with a large attachment coefficient, such as $SF_6$ and $F_2$ have cross section maxima in the electron energy range of 300 – 500 K [27]. These maxima are far from the mean electron energy in self-sustained discharge in nitrogen, and hence the rate constants of electron attachment to $SF_6$ and $F_2$ in the self-sustained discharge are $10^{-9} - 3 \times 10^{-9}$ cm$^3$ s$^{-1}$, while the plasma voltage increases by 30 % – 40 %. Such an increase in voltage is insufficient to produce lasing during the quasi-stationary discharge stage. Figure 7 shows the electron energy distribution function in the $N_2 : NF_3 = 25 : 1$ mixture at $p = 78$ Torr and $U_0 = 35$ kV, as well as the cross section for electron attachment to $NF_3$ and $SF_6$ molecules. The vertical dashed line indicates the mean electron energy in the discharge. One can see that only a small part of low-energy electrons can be attached to $SF_6$, while the maximum of the $NF_3$ cross section quite accurately coincides with the mean electron energy $T_e$. Nevertheless, the two-peak oscillation in a nitrogen laser can also exist with $SF_6$ at a concentration of $\sim 50$ %. Figure 8 demonstrates this lasing for the $N_2 : SF_6 = 12 : 12$ Torr mixture.

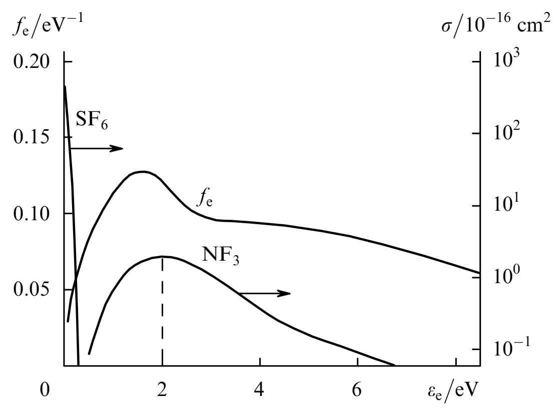


**Figure 7.** Electron energy distribution function in nitrogen for $E/p = 60$ kV cm$^{-1}$ atm$^{-1}$ and the cross sections of electron attachment to $NF_3$ and $SF_6$ molecules.

Numerical calculations showed that the output parameters of the laser strongly depend on all the initial parameters of the experiment: the charge voltage, the parameters of the power supply elements, the initial electron concentration created by the preionisation system, the geometry of the electrodes and the mixture composition. Consider in more detail the effect of the $N_2 - NF_3$ mixture pressure on the laser parameters. Note that the final effect of the variation in the mixture pressure on the yield of coherent radiation is not obvious because, for example, a decrease in pressure causes an increase in the parameter $E/p$ (the pressure decreases while the breakdown voltage changes insignificantly) and in the rate of excitation of the upper laser level. But on the other hand, due to a decrease in the nitrogen pressure and electron concentration in the discharge, the excitation rate of this state should decrease. To

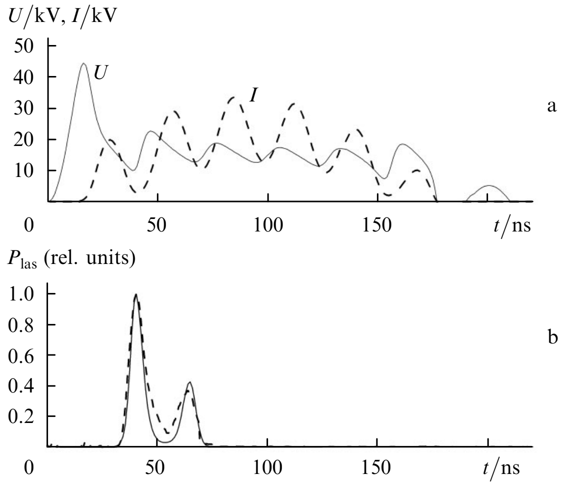


**Figure 8.** Calculated shapes of voltage pulses across the discharge gap and discharge current (a), and the shape of calculated (solid curve) and measured (dashed curve) laser pulses (b) in the mixture $N_2:SF_6 = 12:12$ Torr.

determine the result of the action of these two opposite trends, we calculated numerically the parameters of output laser radiation in the pressure range 15 – 31 Torr for the $N_2 - NF_3$ mixture, which coincided quite well with the experimental results (Fig. 9). The output energy decreases with mixture pressure because in this case the excitation rate of the upper laser level eventually decreases. Thus, the latter of the two opposite trends dominates upon a change in pressure. In addition, we found that the two laser pulse peaks merged into a single peak of duration ~ 40 ns at low pressures (~ 15 Torr) whereas the laser pulse duration in the normal operation regime of the nitrogen laser is 10 ns or less as a rule [1 – 10].

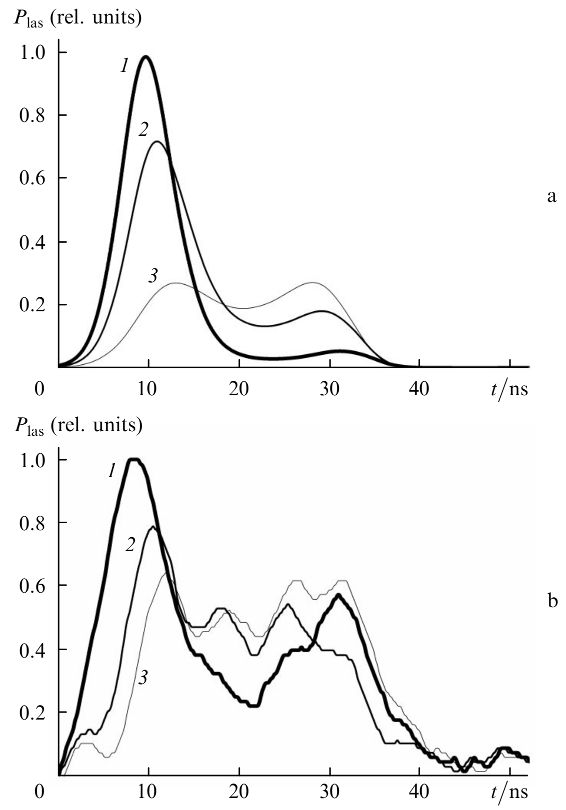


**Figure 9.** Calculated (a) and experimental (b) time dependences of the laser pulse shape for $N_2:NF_3 = 30:1$ mixture at a pressure of 31 (*1*), 21 (*2*) and 15 Torr (*3*).

To find the reasons behind such a discrepancy, we calculated numerically the excitation rates of the lower and upper laser levels, their population inversion and the characteristic time of the photon-concentration evolution in the cavity. Some of the obtained results, which are required for interpreting this effect, are presented in Fig. 10. One can see that the position of the second laser peak weakly changes in time, while the first peak is delayed by 6 ns at $p = 15$ Torr compared to the same peak at a pressure of 30 Torr. Because the width of the laser peaks at the base is 16 ns, they overlap and a single broad trapezoidal peak of total duration 40 ns is formed. The physical interpretation of the effect is that due to the delay of the first laser peak, its maximum coincides with the next pump pulse of the upper laser level, and this sustains lasing over a long period of time.

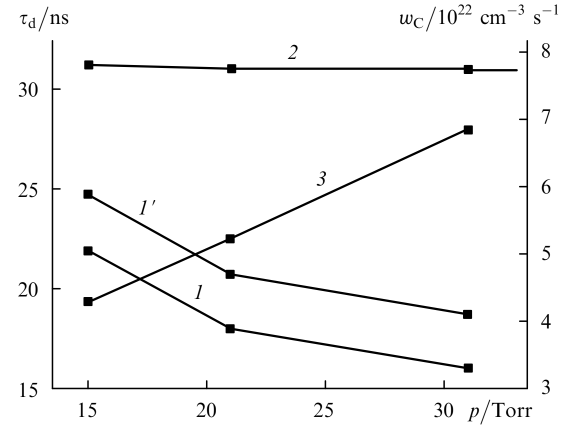


**Figure 10.** Appearance time of the first (*1*, *1'*) and second (*2*) laser peaks as a function of pressure of the $N_2:NF_3 = 30:1$ mixture; curve (*3*) describes the excitation rate for the upper laser level [curves (*1*, *2*) correspond to numerical calculations, while curve (*1'*) is the estimate obtained from (7)].

It follows from our calculations that the 6-ns shift of the first laser pulse is directly caused by a decrease in the excitation rate of the upper electron state $C^3\Pi_u$ and in the population inversion of the laser levels. The second reason is related to a slow evolution of the photon density in the optical cavity during the discharge formation at the beginning of the pump pulse. The initial photon density at the stage of discharge formation in the cavity is low, and its build-up time varies from 10 to 20 ns. Because the photon evolution obeys a nearly exponential law, even a slight decrease in the inversion of laser levels causes a considerable delay in the first laser pulse. After completion of the discharge formation and the establishment of quasi-stationary concentrations of excited molecules, this effect is not so noticeable. For this reason, the displacement of the second peak of the laser pulse is small. This conclusion is confirmed by the approximate estimate of the laser pulse delay from the expression

$$\tau_d = \ln\left(\frac{n_{\mathrm{ph\,m}}}{n_{\mathrm{ph\,0}}}\right)\left(\frac{c}{L}\right)^{-1}\left[\sigma\bar{n}l_a + \frac{\ln(r_1 r_2)}{2}\right]^{-1}, \qquad (7)$$

where $n_{\rm ph\,0}$ and $n_{\rm ph\,m}$ are the initial and maximum photon density in the cavity, and $\bar{n}$ is the mean value of the difference $n_{\rm C} - n_{\rm B}$ in the time interval $\tau_{\rm d}$ under study. Expression (7) can be derived from Eqn (6) by assuming that $n = \rm const$. The values of $\bar{n}$ were obtained from calculations. The numerical values of the delay time for the first laser pulse obtained from (7) differ from the results of numerical simulation, but both curves are identical in shape. Therefore, the displacement $\tau_{\rm d}$ of the first laser peak upon a change in pressure is nearly the same in both cases.

## 6. Conclusions

We have studied experimentally and simulated numerically the operation of a transverse-discharge-pumped nitrogen laser. A theoretical model of a nitrogen – electronegative gas mixture laser has been developed and used for calculating the lasing parameters at the $C^3\Pi_u \rightarrow B^3\Pi_g$ transition upon the addition of electronegative gases $NF_3$ and $SF_6$ to nitrogen, as well as for predicting the conditions for obtaining maximum output energy.

The lasing parameters in $N_2 - NF_3$ and $N_2 - SF_6$ mixtures have been studied experimentally and simulated numerically. It has been shown that in these mixtures the maximum output of the nitrogen laser is achieved and several pulses (usually two) are generated. The second laser pulse appears at the quasi-stationary stage of the discharge due to an increase in the voltage caused by the attachement of electrons to electronegative molecules and due to a large pump pulse duration ($\sim$ 100 ns).

A decrease in the mixture pressure results in an increase in the delay in the first emission peak of the nitrogen laser with respect to the second one, the other conditions remaining the same. In this case, both laser peaks coincide so that a single laser pulse of duration up to 40 – 50 ns is formed during pumping.

***Acknowledgements.*** This work was supported by the International Science and Technology Center (Project No. 2596).

## References

1. Levatter J.I., Lin S.-C. *Appl. Phys. Lett.*, **25**, 703 (1974).
2. Suchard S.I., Galvan L., Sutton D.G. *Appl. Phys. Lett.*, **26**, 521 (1975).
3. Losev V.F., Tarasenko V.F. *Zh. Tekh. Fiz.*, **46**, 2202 (1976).
4. Rebhan U., Hildebrandt J., Skopp G.A. *Appl. Phys. A: Mater. Sci. & Proc.*, **23**, 341 (1980).
5. Armandillo E., Kearsley A.J. *Appl. Phys. Lett.*, **41**, 611 (1982).
6. Buranov S.N., Gorokhov V.V., Karelin V.I., Repin P.B. *Kvantovaya Elektron.*, **17**, 161 (1990) [*Sov. J. Quantum Electron.*, **20**, 120 (1990)].
7. Lomaev M.I., Tarasenko V.F., Verkhovskii V.S. *Elektron. Tekhn. Lazer. Tekhn. Optoelektron.*, No. 1 (57), 58 (1991).
8. Tzolov V.P., Grozdanov K.A., Atanasov P.A. *J. Appl. Phys.*, **75**, 1210 (1994).
9. Apollonov V.V., Yamshchikov V.A. *Kvantovaya Elektron.*, **24**, 483 (1997) [*Quantum Electron.*, **27**, 469 (1997)].
10. Tarasenko V.F. *Kvantovaya Elektron.*, **31**, 489 (2001) [*Quantum Electron.*, **31**, 489 (2001)].
11. Alekseev S.B., Baksht E.Kh., Kostyrya I.D., Orlovskii V.M., Panchenko A.N., Tarasenko V.F. *Kvantovaya Elektron.*, **34**, 1033 (2004) [*Quantum Electron.*, **34**, 1033 (2004)].
12. Panchenko A.N., Tarasenko V.F., Tel'minov A.E. *Opt. Atmos. Okean.*, **19**, 158 (2006).
13. Ali A.W., Kolb A.C., Anderson A.D. *Appl. Opt.*, **6**, 2115 (1967).
14. Bychkov Yu.I., Losev V.F., Savin V.V., Tarasenko V.F. *Kvantovaya Elektron.*, **2**, 2047 (1975) [*Sov. J. Quantum Electron.*, **5**, 1111 (1975)].
15. Makuchovsky J., Pokora L. *Optica Applicata*, **23**, 113 (1993).
16. Makuchovsky J., Pokora L. *Optica Applicata*, **23**, 131 (1993).
17. Makuchovsky J., Pokora L. *Optica Applicata*, **23**, 217 (1993).
18. Panchenko A.N., Tarasenko V.F., Tel'minov A.E. *Kvantovaya Elektron.*, **36**, 403 (2006) [*Quantum Electron.*, **36**, 403 (2006)].
19. Sanz F.E., Perez J.M.G. *Appl. Phys. B*, **52**, 42 (1991).
20. Fortov V.E. (Ed.) *Entsiklopedia nizkotemperaturnoi plazmy* (Encyclopaedia of Low-temperature Plasma) (Moscow: Nauka, 2000).
21. Itikawa Y., Hayashi M., Ichimura A., et al. *J. Phys. Chem. Ref. Data*, **15**, 985 (1986).
22. Kalyuzhnaya A.G., Ryabtsev A.V., Shchedrin A.I. *Zh. Tekh. Fiz.*, **73**, 42 (2003).
23. Herron J.T. *J. Phys. Chem. Ref. Data*, **28**, 1453 (1999).
24. Smirnov B.M. (Ed.) *Khimiya plazmy* (Plasma Chemistry) (Moscow: Energoatomizdat, 1983) Vol. 10, p. 108.
25. Kossyi I.A., Kostinskii A.Yu., Matveev A.A., Silakov V.P. *Trudy IOFAN*, **47**, 37 (1994).
26. Nandi D., Rangwala S.A., Kumar S.V.K., Krishnakumar E. *Int. J. Mass Spectrometry*, **205**, 111 (2001).
27. Christophorou L.G., Olthoff J.K. *Int. J. Mass Spectrometry*, **205**, 27 (2001).